JACS
JOURNAL OF THE AMERICAN CHEMICAL SOCIETY

COMMUNICATION

pubs.acs.org/JACS

Thermodynamics and Selectivity of Two-Dimensional Metallo-supramolecular Self-Assembly Resolved at Molecular Scale

Ziliang Shi,[†] Jun Liu,[‡] Tao Lin,[†] Fei Xia,[‡] Pei Nian Liu,*[,‡] and Nian Lin*[,†]

[†]Department of Physics, The Hong Kong University of Science and Technology, Clear Water Bay, Hong Kong, China

[‡]Key Lab for Advanced Materials and Institute of Fine Chemicals, East China University of Science and Technology, Meilong Road 130, Shanghai, China

Supporting Information

ABSTRACT: We investigated the thermodynamic processes of two-dimensional (2D) metallo-supramolecular self-assembly at molecular resolution using scanning tunneling microscopy and variable-temperature low-energy electron diffraction. On a Au(111) substrate, tripyridyl ligands coordinated with Cu in a twofold Cu−pyridyl binding mode or with Fe in a threefold Fe−pyridyl binding mode, forming a 2D open network structure in each case. The network structures exhibited remarkable thermal stability (600 K for the Cu-coordinated network and 680 K for the Fe-coordinated network). The Fe−pyridyl binding was selected thermodynamically as well as kinetically in self-assembly involving both modes. The selectivity can be effectively suppressed in a specifically designed self-assembly route.

This report describes a single-molecule-resolution study of the self-assembly thermodynamics and selectivity of two-dimensional (2D) metallo-supramolecular systems. Supramolecular self-assembly is a highly complex and dynamic process. Particularly, in systems with competing binding modes, thermodynamic or kinetic selectivity among many possible alternatives decides the pathway leading to the output structure.[1−6] In recent years, the concept of 2D supramolecular self-assembly (i.e., at solid−liquid or solid−vacuum interfaces) has been introduced.[7−11] In contrast to 3D self-assembly, fewer degrees of freedom are available for molecules and atoms confined at interfaces. Furthermore, the self-assembly process and the structures that are formed at interfaces are both subject to molecule−substrate and atom−substrate interactions.[9−11] These unique features are expected to bring distinctive thermodynamic characteristics, and thus, an in-depth investigation of the thermodynamics of 2D supramolecular self-assembly is highly desirable and may allow for the design of complex low-dimensional supramolecular structures having desired properties and functionality.

Here we report that on a Au(111) surface, molecular ligands of 1,3,5-tris(pyridyl)benzene (TPyB, shown in Scheme 1) assemble with Cu or Fe, forming twofold Cu−py (py = pyridyl) coordination or threefold Fe−py coordination. The self-assembly processes are reversible, and the thermodynamic equilibria were assessed by the binding constants K_{Cu} and K_{Fe}. When both Cu and Fe are engaged in the self-assembly, the Fe−py coordination is selected both thermodynamically and kinetically.

Figure 1a is a representative scanning tunneling microscopy (STM) topograph of the honeycomb structure formed by Cu and TPyB. The STM image clearly reveals that two adjacent molecules point toward each other collinearly. Considering the repulsive force between the two terminal py groups, we propose that twofold linear

Scheme 1. Schematic Representation of Self-Assembly Pathways Involving Different Binding Modes

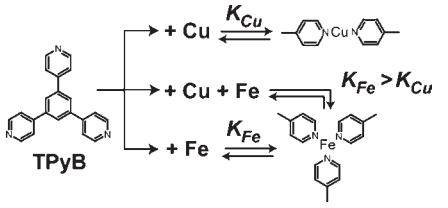

py−Cu−py coordination stabilizes the honeycomb network structure,[12−14] as illustrated by the structural model in Figure 1b. The lattice constant of the network (see the rhombus unit cell in Figure 1a) is 2.73 ± 0.05 nm. In large-scale STM images, (see Figure S1 in the Supporting Information) network domains with two different orientations were identified. The angle between the two domain orientations was 28 ± 2°, as estimated from the STM topographs as well as Fourier transforms of the large-scale images (Figure 1c). A low-energy electron diffraction (LEED) pattern of the TPyB−Cu network acquired at room temperature (293 K) is shown in Figure 1d. This LEED pattern reproduced the signatures of the Fourier transform.[15,16] The LEED data infer that the network periodicity is 2.76 ± 0.05 nm and that the networks are oriented at an angle of 14 ± 2° with respect to the $\langle 11\bar{2} \rangle$ direction of the Au(111) surface lattice. The structural characteristics determined by LEED agree fairly well with the STM results.

To investigate the dynamic process of the self-assembly, we acquired a series of LEED data as the samples were annealed to higher temperatures. Figure 1e,f shows two snapshots of such a series, acquired at sample temperatures of 571 and 643 K, respectively. It can be seen that the diffraction pattern is still recognizable at 571 K but unrecognizable at 643 K. As the mean network domain size (~50 nm; see Figure S1) was larger than the beam coherence length (~10 nm) and much smaller than the beam size (~2 mm), the diffraction spot intensity was related to the total area of the network phase.[17−19] Figure 1g displays the line profiles of the diffraction intensity along the (0,1) direction as a function of sample temperature, providing a temperature-dependent monitor of the evolution of the networks. Figure 1g shows that the signature of the (0,1) spot becomes weak at elevated temperatures and vanishes above 600 K, indicating shrinkage of the total network area at elevated temperatures and complete dissolution of the networks at 600 K. It is known that

Received: February 2, 2011
Published: April 05, 2011

dx.doi.org/10.1021/ja2010434 | J. Am. Chem. Soc. 2011, 133, 6150–6153

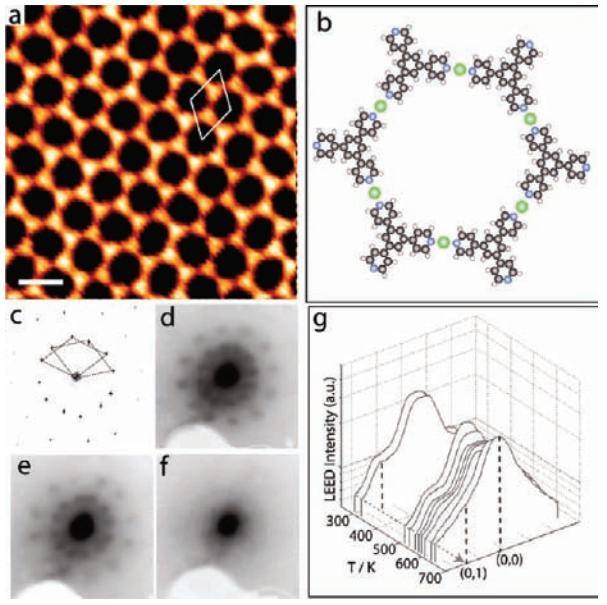

Figure 1. (a) STM topograph of the TPyB−Cu network (scale bar: 3 nm). (b) Structural model of the TPyB−Cu network (Cu in green and N in blue). (c) Fourier transform of the large-scale STM data. The rhombus frames show the two sets of diffraction spots. (d−f) LEED (15 eV) patterns of the TPyB−Cu phase acquired at 293, 571, and 643 K, respectively. (g) LEED intensity profiles along the (0,1) direction as a function of sample temperature.

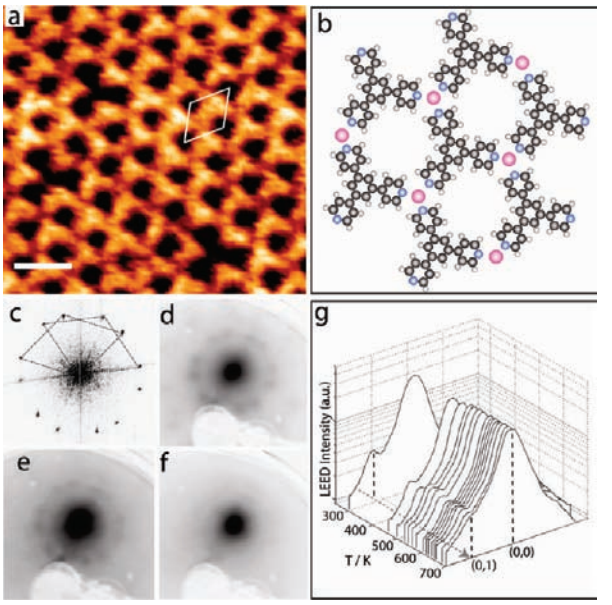

Figure 2. (a) STM topograph of the TPyB−Fe network (scale bar: 2 nm). (b) Structural model of the TPyB−Fe network (Fe in purple and N in blue). (c) Fourier transform of the large-scale STM data. The rhombus frames show the two sets of diffraction spots. (d−f) LEED (20 eV) patterns of the TPyB−Fe phase acquired at 293, 653, and 693 K, respectively. (g) LEED intensity profiles along the (0,1) direction as a function of sample temperature.

porous coordination materials are thermally less stable than inorganic materials because of the presence of the coordination bonds. Framework structures typically are not stable above 500 K, except for a few examples exhibiting greater thermal stability.[20−23] As the 2D TPyB−Cu system consisted of only one layer of coordination network, its thermal stability up to 600 K was remarkably high.[24]

The gradual reduction of the network area is a manifestation of the reversible self-assembly process in which the TPyB molecules are in a thermodynamic equilibrium between incorporation in the networks via Cu coordination and being in the molecular phase.[25−28] This process can be described by the equation Cu + TPyB $\rightleftarrows$ TPyB−Cu, where TPyB and TPyB−Cu refer to the free and Cu-bound molecular species, respectively. The affinity of TPyB−Cu coordination is related to the binding constant K_{Cu}, which assesses the thermodynamic equilibrium of the self-assembly process. The binding constant can be evaluated from the concentrations of the coordinated and noncoordinated TPyB molecules present on the surface: $K_{Cu} = [\text{TPyB−Cu}]/([\text{TPyB}][\text{Cu}])$. Under our experimental conditions, Cu was always overdosed (as indicated by the Cu islands grown at the Au(111) step edges; see Figure S2), so [Cu] is the 2D vaporized adatom gas density, which increases exponentially with temperature. The concentration of the free molecules is $[\text{TPyB}]_0 - [\text{TPyB−Cu}]$, where $[\text{TPyB}]_0$ is the total molecule density given by deposition. The concentration of the coordinated molecules, [TPyB−Cu], is proportional to the total area of the TPyB−Cu networks, which is related to the intensity of the LEED (0,1) spot. Hence, Figure 1g implies that [TPyB−Cu] decreases at elevated temperatures and reaches a very low value (below the LEED detection limit) above 600 K. Thus, the numerator (denominator) in the binding constant expression is reduced (enlarged) at elevated temperatures, indicating that the binding constant decreases with increasing temperature and reaches a minimum value above 600 K. This behavior is in accordance with the van't Hoff equation.

A different type of network was observed as Fe atoms were codeposited with TPyB on the surface. As shown in a representative STM topograph (Figure 2a), this structure is a triangular network in which three adjacent molecules are linked through their terminal py groups in a trigonal manner. The structural model (Figure 2b) shows three py ligands coordinated by a central Fe atom in a threefold trigonal configuration. The rhombus frame in Figure 2a denotes the unit cell of the TPyB−Fe triangular lattice with a lattice constant of 1.40 ± 0.05 nm. The Fourier transform of the large-scale STM images (Figure 2c) shows network domains having two different orientations at an angle of $22 \pm 2°$. A LEED pattern of the TPyB−Fe networks acquired at room temperature (Figure 2d) resembles the Fourier transform. Again, the LEED- and STM-resolved structural characteristics agree with each other very well. Figure 2e,f shows two snapshots of LEED data in a heating series of the TPyB−Fe networks at 653 and 693 K, respectively. The LEED pattern is recognizable at 653 K, indicating that this structure can survive a higher temperature than the TPyB−Cu networks. Figure 2g shows the line profiles of the diffraction intensity along the (0,1) direction as a function of sample temperature. The intensity reduction of the (0,1) spot at elevated temperatures is less dramatic than for the TPyB−Cu structure, implying that the rate of decrease in the total network area at higher temperatures is lower. The networks are thermally stable up to ~680 K, about 80 degrees higher than for the TPyB−Cu phase. Similarly, the self-assembly process can be described as Fe + TPyB $\rightleftarrows$ TPyB−Fe, and the binding constant is $K_{Fe} = [\text{TPyB−Fe}]/([\text{TPyB}][\text{Fe}])$. The LEED data imply that (1) K_{Fe} decays more slowly at elevated temperatures than K_{Cu} and (2) K_{Fe} reaches the minimum at a temperature 80 degrees higher than that for K_{Cu}.

To study the selectivity in the self-assembly involving both binding modes, we prepared samples in which TPyB molecules were deposited with a mixture of Fe and Cu according to two different deposition sequences.[29] The first sequence (denoted as S-I) involved deposition of Cu and Fe first and then TPyB. The second sequence

dx.doi.org/10.1021/ja2010434 |J. Am. Chem. Soc. 2011, 133, 6150–6153

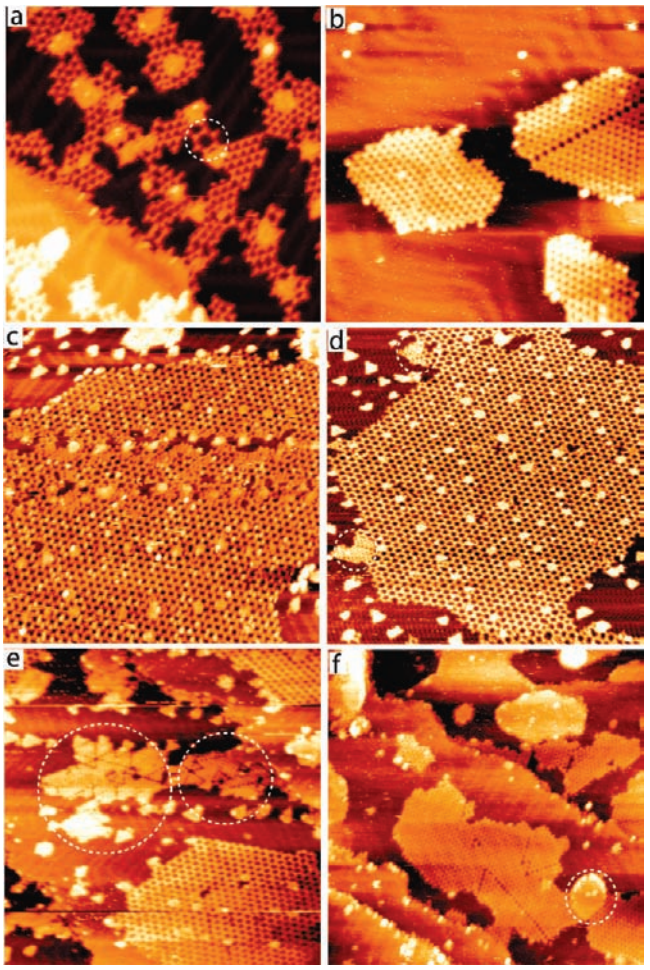

Figure 3. STM topographs (a and b, 50 nm × 50 nm; c−f, 100 nm × 100 nm) of the sample prepared by depositing TPyB onto a mixture of Cu and Fe (a) at 293 K (the circle highlights a TPyB−Cu honeycomb unit) and (b) after annealing at 400 K. STM topographs of the sample prepared by depositing Fe onto a preformed TPyB−Cu phase (c) at 293 K, (d) after annealing at 410 K, (e) after annealing at 450 K (circles highlight the TPyB−Fe networks with the characteristic defect lines), and (f) after annealing at 500 K (the circle marks a Cu island).

(denoted as S-II) involved initial deposition of Cu and TPyB, annealing to form the large TPyB−Cu networks, and lately deposition of Fe. After STM characterizations, the samples were annealed step-by-step at higher temperatures, and after each annealing step, the samples were characterized by STM. As Figure 3 shows, different network structures (e.g., a mixture of TPyB−Cu and TPyB−Fe, pure TPyB−Cu, or pure TPyB−Fe) were observed depending on the deposition sequence and annealing temperature.

Figure 3a,c shows representative STM topographs of S-I and S-II samples, respectively, without any annealing. On the S-I sample, the TPyB molecules were predominantly incorporated in the TPyB−Fe phase, with only a very few in the TPyB−Cu phase (see the circled area in Figure 3a). In contrast, on the S-II sample (Figure 3c), most of the TPyB molecules were incorporated in the TPyB−Cu phase, while the Fe atoms nucleated into small islands on the bare Au substrate as well as inside the TPyB−Cu honeycomb networks. Detailed inspection revealed that in both regions, Fe islands decorated the elbow sites of the herringbone reconstruction of Au(111). This observation suggests that the randomly deposited Fe atoms diffuse freely through the TPyB−Cu networks without damaging the network motifs.[30] After the samples were annealed at 400 K or higher temperatures, only the TPyB−Fe phase was present on the S-I sample (Figure 3b). Similarly, the pure TPyB−Fe phase was present on the S-II sample after annealing at higher temperatures (∼500 K) (Figure 3f). Thus, independent of the deposition sequence, the final structure after the high-temperature annealing was always the pure TPyB−Fe phase. It should be noted that on both samples, Cu islands were present after the high-temperature annealing (see the circle in Figure 3f), excluding the possibility that formation of the TPyB−Fe phase was due to Cu deficiency. Since the thermodynamic equilibrium was reached after the high-temperature annealing, one can conclude that the Fe−py binding mode is thermodynamically selected.

On the other hand, the existence of the TPyB−Cu phase at 293 K in Figure 3c indicates that the self-assembly processes did not reach the equilibrium at this temperature and hence were controlled by the kinetic selectivity. On the S-I sample, both Cu and Fe were present as the TPyB molecules were deposited, so the rate constants for Cu−py binding and Fe−py binding determined which phase was selected. A statistical analysis of the STM data for the S-I sample found that at 293 K, the number of TPyB molecules incorporated into the TPyB−Fe phase was ∼9 times that in the TPyB−Cu phase. As the concentration of free molecules, [TPyB], was same for both coordination processes, we estimate that the rate constant for Fe−py binding is about three orders of magnitude larger than that for Cu−py binding (the bulk (3D) vapor pressure of Cu is 3−4 orders of magnitude higher than that of Fe at same temperature.[31,32] On a surface, the [Cu]/[Fe] ratio can be approximately estimated as the two-thirds power of the bulk ratio because there are only two dimensions, giving rise to a [Cu]/[Fe] ratio larger than 100.)

Thermodynamically favored processes can be inhibited kinetically by invoking kinetic control.[33,34] This effect was clearly manifested on the S-II sample, where the thermodynamically and kinetically less-favored TPyB−Cu binding was artificially formed first by adjusting the deposition sequence. Figure 3c reveals that at 293 K, the preformed TPyB−Cu phase was almost unchanged after introduction of Fe, indicating that the dissociation of the Cu−py binding is very slow, significantly hindering the Fe−py binding even though the latter is the thermodynamically and kinetically favored mode. Figure 3d−f shows the STM topographs of the sample annealed at 410, 450, and 500 K, respectively. After annealing at 410 K, small islands of the TPyB−Fe phase could be identified (marked by the circles in Figure 3d), while most of the molecules were still in the TPyB−Cu phase. After annealing at 450 K, the area of the TPyB−Fe networks (see the islands circled in Figure 3e) increased (containing roughly half of TPyB molecules), whereas the TPyB−Cu networks contained the rest of molecules. After annealing at 500 K, the TPyB−Cu networks vanished, and only the TPyB−Fe networks were present.

The structural evolution of the S-II sample at different annealing temperatures was also monitored by LEED. Figure 4a−c shows the typical LEED patterns acquired at 293, 449, and 549 K, respectively. These data imply that the TPyB−Cu phase was preserved at 449 K and that at 549 K the TPyB−Cu phase disappeared but the TPyB−Fe phase remained. Figure 4d is a LEED pattern acquired as the sample was cooled down to room temperature; it shows the signatures of the TPyB−Fe phase only. Figure 4e,f shows line profiles of the diffraction intensities along the (0,1) direction of the two phases as functions of temperature. The TPyB−Cu (0,1) spot gradually decreases with increasing temperature but is still recognizable up to 490 K. The TPyB−Fe (0,1) spot is recognizable up to the

dx.doi.org/10.1021/ja2010434 |J. Am. Chem. Soc. 2011, 133, 6150–6153

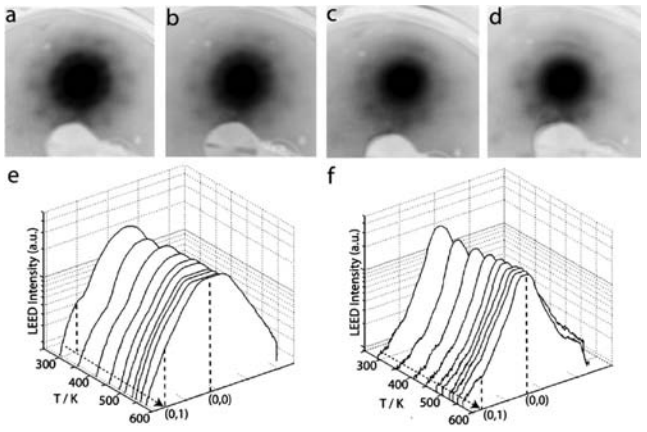

Figure 4. (a−d) LEED (a and b, 15 eV; c and d, 20 eV) patterns of the sample prepared by depositing Fe onto a preformed TPyB−Cu phase (a) at 293 K, (b) at 449 K, (c) at 549 K, and (d) after cooling to 293 K. (e, f) LEED intensity profiles along the (0,1) direction for the (e) TPyB−Cu and (f) TPyB−Fe phases as functions of sample temperature.

highest annealing temperature, 570 K. These data indicate that the transformation from the TPyB−Cu phase to the TPyB−Fe phase was complete at ∼490 K, which is ∼90 degrees higher than in the self-assembly of the S-I sample. Therefore, the selectivity to form TPyB−Fe is effectively suppressed along this self-assembly route. In addition, the LEED data also reveal the notable fact that the presence of Fe reduces the thermal stability of the TPyB−Cu networks from ∼600 to ∼490 K. This phenomenon can be attributed to the fact that the Fe atoms shift the equilibrium of the TPyB−Cu self-assembly toward the dissociation side: as the free TPyB molecules are consumed by incorporation into the TPyB−Fe networks, the free molecule concentration [TPyB] is reduced; therefore, [TPyB−Cu] is reduced at given values of the binding constant K_{Cu} and the Cu concentration [Cu].

In summary, we have investigated the temperature-dependent structural evolution of the 2D supramolecular self-assembly for two different binding modes and their competive binding. We have found that the Fe−py binding is selected over the Cu−py binding both thermodynamically and kinetically. We have also demonstrated that the selectivity can be suppressed by manipulating the self-assembly route. Finally, we note that in systems where metal atoms undergo appreciable desorption, bulk diffusion, or cluster formation, this technique cannot provide accurate information about the self-assembly dynamics.

■ ASSOCIATED CONTENT

Supporting Information. Detailed experimental procedures, including sample preparation and STM and LEED measurements, and additional STM images. This material is available free of charge via the Internet at http://pubs.acs.org.

■ AUTHOR INFORMATION

Corresponding Author
liupn@ecust.edu.cn; phnlin@ust.hk

■ ACKNOWLEDGMENT

This work was financially supported by the Hong Kong RGC (Grants 602008 and 602409), the NSFC (Project 20902020), and the Shanghai Pujiang Talent Program (Project 09PJ1403500).

■ REFERENCES

(1) Atwood, J. L.; Davies, J. E. D.; MacNicol, D. D.; Vögtle, F.; Lehn, J.-M. *Comprehensive Supramolecular Chemistry*; Pergamon: New York, 1996.
(2) Lehn, J.-M. *Supramolecular Chemistry: Concepts and Perspectives*; VCH: Weinheim, Germany, 1995.
(3) Steed, J. W.; Atwood, J. L. *Supramolecular Chemistry*; Wiley-VCH: Weinheim, Germany, 2000.
(4) Saalfrank, R. W.; Demleitner, B. In *Transition Metals in Supramolecular Chemistry*; Sauvage, J.-P., Ed.; *Perspectives in Supramolecular Chemistry*, Vol. 5; Wiley: Chichester, U.K., 1999; pp 1−51.
(5) Davis, A. V.; Yeh, R. M.; Raymond, K. N. *Proc. Natl. Acad. Sci. U.S.A.* **2002**, *99*, 4793.
(6) Holliday, B. J.; Mirkin, C. A. *Angew. Chem., Int. Ed.* **2001**, *40*, 2022.
(7) De Feyter, S.; De Schryver, F. C. *Chem. Soc. Rev.* **2003**, *32*, 139.
(8) De Feyter, S.; De Schryver, F. C. *J. Phys. Chem. B* **2005**, *109*, 4290.
(9) Barth, J. V. *Annu. Rev. Phys. Chem.* **2007**, *58*, 375.
(10) Lin, N.; Stepanow, S.; Ruben, M.; Barth, J. V. *Top. Curr. Chem.* **2009**, *287*, 1.
(11) Stepanow, S.; Lin, N.; Barth, J. V. *J. Phys: Condens. Matter* **2008**, *20*, No. 184002.
(12) Tait, S. L.; Langner, A.; Lin, N.; Stepanow, S.; Rajadurai, C.; Ruben, M.; Kern, K. *J. Phys. Chem. C* **2007**, *111*, 10982.
(13) Shi, Z.; Lin, N. *ChemPhysChem* **2010**, *11*, 97.
(14) Klappenberger, F.; Weber-Bargioni, A.; Auwärter, W.; Marschall, M.; Schiffrin, A.; Barth, J. V. *J. Chem. Phys.* **2008**, *129*, No. 214702.
(15) Matena, M.; Stöhr, M.; Riehm, T.; Björk, J.; Martens, S.; Dyer, M. S.; Persson, M.; Lobo-Checa, J.; Müller, K.; Enache, M.; Wadepohl, H.; Zegenhagen, J.; Jung, T. A.; Gade, L. H. *Chem.—Eur. J.* **2010**, *16*, 2079.
(16) Tseng, T.-C.; Lin, C.; Shi, X.; Tait, S. L.; Liu, X.; Starke, U.; Lin, N.; Zhang, R.; Minot, C.; Van Hove, M. A.; Cerdá, J. I.; Kern, K. *Phys. Rev. B* **2009**, *80*, No. 155458.
(17) Lagally, M. G. *Appl. Surf. Sci.* **1982**, *13*, 260.
(18) Pfnür, H.; Voges, C.; Budde, K.; Lyuksyutov, I.; Everts, H.-U. *J. Phys.: Condens. Matter* **1999**, *11*, 9933.
(19) Lu, T. M.; Wang, G. C.; Lagally, M. G. *Phys. Rev. Lett.* **1977**, *39*, 411.
(20) Kitagawa, S.; Kitaura, R.; Noro, S. *Angew. Chem., Int. Ed.* **2004**, *43*, 2334.
(21) Li, H.; Eddaoudi, M.; O'Keeffe, M.; Yaghi, O. M. *Nature* **1999**, *402*, 276.
(22) Yaghi, O. M.; O'Keeffe, M.; Ockwig, N. W.; Chae, H. K.; Eddaoudi, M.; Kim, J. *Nature* **2003**, *423*, 705.
(23) Park, K. S.; Ni, Z.; Cote, A. P.; Choi, J. Y.; Huang, R.; Uribe-Romo, F. J.; Chae, H. K.; O'Keeffe, M.; Yaghi, O. M. *Proc. Natl. Acad. Sci. U.S.A.* **2006**, *103*, 10186.
(24) Kühne, D.; Klappenberger, F.; Decker, R.; Schlickum, U.; Brune, H.; Klyatskaya, S.; Ruben, M.; Barth, J. V. *J. Am. Chem. Soc.* **2009**, *131*, 3881.
(25) Yanagi, H.; Mukai, H.; Ikuta, K.; Shibutani, T.; Kamikado, T.; Yokoyama, S.; Mashiko, S. *Nano Lett.* **2002**, *2*, 601.
(26) Lin, N.; Dmitriev, A.; Weckesser, J.; Barth, J. V.; Kern, K. *Angew. Chem., Int. Ed.* **2002**, *41*, 4779.
(27) Berner, S.; De Wild, M.; Ramoino, L.; Ivan, S.; Baratoff, A.; Güntherodt, H.-J.; Suzuki, H.; Schlettwein, D.; Jung, T. A. *Phys. Rev. B* **2003**, *68*, No. 115410.
(28) Berner, S.; Brunner, M.; Ramoino, L.; Suzuki, H.; Güntherodt, H.-J.; Jung, T. A. *Chem. Phys. Lett.* **2001**, *348*, 175.
(29) Langner, A.; Tait, S. L.; Lin, N.; Rajadurai, C.; Ruben, M.; Kern, K. *Proc. Natl. Acad. Sci. U.S.A.* **2007**, *104*, 17927.
(30) Decker, R.; Schlickum, U.; Klappenberger, F.; Zoppellaro, G.; Klyatskaya, S.; Ruben, M.; Barth, J. V.; Brune, H. *Appl. Phys. Lett.* **2008**, *93*, No. 243102.
(31) Ferguson, F. T.; Nuth, J. A., III; Johnson, N. M. *J. Chem. Eng. Data* **2004**, *49*, 497.
(32) Hersh, H. N. *J. Am. Chem. Soc.* **1953**, *75*, 1529.
(33) Hasenknopf, B.; Lehn, J.-M.; Boumediene, N.; Dupont-Gervais, A.; Van Dorsselaer, A.; Kneisel, B.; Fenske, D. *Angew. Chem., Int. Ed.* **1998**, *37*, 3265.
(34) Levin, M. J.; Stang, P. J. *J. Am. Chem. Soc.* **2000**, *122*, 7428.